

Short-range correlations and shell structure of medium-mass nuclei

L. Coraggio,¹ A. Covello,^{1,2} A. Gargano,¹ N. Itaco,^{1,2} and T. T. S. Kuo³

¹*Istituto Nazionale di Fisica Nucleare,*

Complesso Universitario di Monte S. Angelo, Via Cintia - I-80126 Napoli, Italy

²*Dipartimento di Scienze Fisiche, Università di Napoli Federico II,*

Complesso Universitario di Monte S. Angelo, Via Cintia - I-80126 Napoli, Italy

³*Department of Physics, SUNY, Stony Brook, New York 11794, USA*

(Dated: October 26, 2018)

The single-particle spectrum of the two nuclei ^{133}Sb and ^{101}Sn is studied within the framework of the time-dependent degenerate linked-diagram perturbation theory starting from a class of onshell-equivalent realistic nucleon-nucleon potentials. These potentials are derived from the CD-Bonn interaction by using the so-called $V_{\text{low-k}}$ approach with various cutoff momenta. The results obtained evidence the crucial role of short-range correlations in producing the correct $2s1d0g0h$ shell structure.

PACS numbers: 21.30.Fe, 21.60.Cs, 21.10.Pc, 27.60.+j

I. INTRODUCTION

Shell structure plays a key role in explaining many features of atomic nuclei. In particular, the energy gap between groups of levels is crucial in determining their stability properties. However, what is the microscopic origin of the shell structure is still a subject of great theoretical interest.

In recent years special attention has been focused on the role of the various components of the nuclear force in the formation and evolution of the shell structure. This is mainly related to the advent of new advanced techniques and facilities, and in particular to the development of radioactive ion beams, which allow to study how the properties of nuclei may change when going toward the proton or neutron drip line. It is for instance a current matter of investigation the influence of the tensor force on the single-nucleon energies, especially in the case of exotic nuclei [1, 2, 3], where it is expected to produce a reduction of the spin-orbit splitting [4]. This aspect is also discussed in Ref. [5] along with the influence of many-body correlations and of states unbound to particle emission on the single-particle spectrum of neutron-rich nuclei.

In this work, we have studied the structure of the $2s1d0g0h$ -shell for protons and neutrons, calculating the single-particle spectrum of ^{133}Sb and ^{101}Sn with realistic nucleon-nucleon (NN) potentials. Both these nuclei are far from stability, ^{133}Sb having a large neutron excess and ^{101}Sn lying very close to the proton drip line. On the other hand, ^{132}Sn shows strong shell closures for both protons and neutrons while this is not the case for ^{100}Sn , which may imply different core polarization effects on ^{133}Sb and ^{101}Sn . We shall see that the softness of the core plays an important role in the perturbative description of the single-particle structure of these nuclei.

The two nuclei are described as a doubly-closed core plus one valence nucleon, whose correlations with the core are taken into account by means of the time-dependent degenerate linked-diagram perturbation theory [6]. In previous works, single-particle valence nuclei

of the sd -shell have been extensively studied within the same framework by other authors [7, 8, 9]. However, the presence of the intruder state $0h_{11/2}$ makes a more challenging problem to reproduce the structure of the $2s1d0g0h$ -shell.

We have employed a class of onshell-equivalent realistic NN potentials, derived from the CD-Bonn interaction [10] by way of the so-called $V_{\text{low-k}}$ approach [11]. This approach is a very valuable tool since, by varying the cutoff momentum Λ , it provides different NN potentials defined up to Λ which are all onshell equivalent. This allows to study how the short-range (high-momentum) components of the NN potential contribute to determine the nuclear shell structure.

The paper is organized as follows. In Sec. II we give an outline of our calculations, focusing attention on the time-dependent degenerate linked-diagram expansion. Sec. III is devoted to the presentation and discussion of our results for the ^{133}Sb and ^{101}Sn single-particle spectra. Some concluding remarks are given in Sec. IV.

II. OUTLINE OF CALCULATIONS

As mentioned in the Introduction, we calculate the single-particle energies of ^{133}Sb and ^{101}Sn within the framework of the time-dependent degenerate linked-diagram expansion [6, 12]. This means that we describe the wave function of each nucleus as a single-nucleon state $|j\rangle$, whose energy ϵ^j is calculated taking into account perturbatively the interaction of the odd nucleon with the closed core. As a starting point, an auxiliary one-body potential U is introduced to break up the hamiltonian as the sum of an unperturbed term H_0 , which describes the independent motion of the nucleons, and a residual interaction H_1 :

$$\begin{aligned}
H &= \sum_{i=1}^A \frac{p_i^2}{2m} + \sum_{i<j} V_{NN}^{ij} = T + V_{NN} = \\
&= (T + U) + (V_{NN} - U) = H_0 + H_1 . \quad (1)
\end{aligned}$$

The effective single-particle energies are expressed by way of the folded-diagram expansion in terms of the so-called \hat{Q} box:

$$\epsilon^j = \epsilon_0^j + \hat{Q} - \hat{Q}' \int \hat{Q} + \hat{Q}' \int \hat{Q} \int \hat{Q} - \hat{Q}' \int \hat{Q} \int \hat{Q} \int \hat{Q} + \dots , \quad (2)$$

ϵ_0^j being the unperturbed energy of the single-particle state $|j\rangle$, i.e.

$$H_0|j\rangle = (T + U)|j\rangle = \epsilon_0^j|j\rangle . \quad (3)$$

Eq. (2) represents the well known Kuo-Lee-Ratcliff (KLR) folded-diagram expansion [6, 12]. This expansion is written in terms of the vertex function \hat{Q} -box, which is composed of one-body irreducible valence-linked Goldstone diagrams. Once the \hat{Q} -box has been calculated through a certain order in the input interaction V_{NN} , the series of the folded diagrams is summed up to all orders using the Lee-Suzuki iteration method [13].

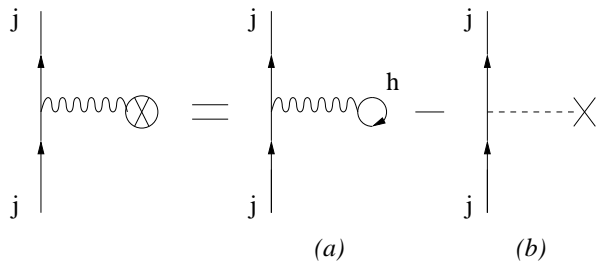


FIG. 1: First-order diagram. Graph (a) is the so-called self-energy diagram. Graph (b) represents the matrix element of the harmonic oscillator potential $U = \frac{1}{2}m\omega r^2$.

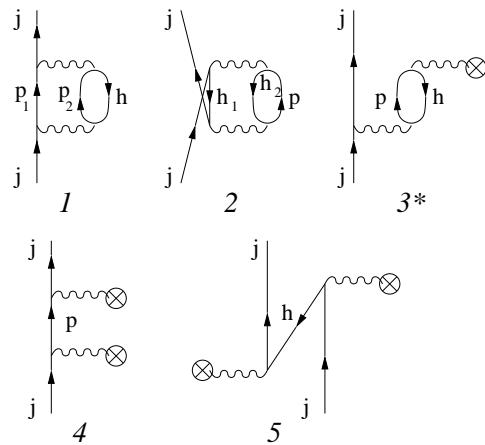


FIG. 2: Second-order diagrams. The asterisk indicates non-symmetric diagrams, which occur always in pairs giving equal contributions. For the sake of simplicity we report only one of them.

Our calculations have been performed including all the one-body irreducible valence-linked Goldstone diagrams up to third order in V_{NN} . In Fig. 1 the first-order diagram, which is composed of the so-called self-energy diagram, minus the auxiliary potential U -insertion, is reported while the second- and third-order diagrams are shown in Figs. 2 and 3, respectively. The U -insertion diagrams arise in the perturbative expansion owing to the presence of the $-U$ term in H_1 (see Eq. (1)). In our calculation we have used as auxiliary potential the harmonic oscillator (HO) one, which is the most common choice.

Let us now focus our attention on the input interaction V_{NN} . Of course, it would be very desirable to use directly a realistic NN potential that reproduces with high precision the two-body scattering data and deuteron properties. However, to perform nuclear structure calculations in a perturbative framework with realistic NN potentials one has first to deal with the strong repulsive behavior of such potentials in the high-momentum regime. An advantageous method to renormalize the bare NN interaction has been proposed in [11, 14]. It consists in deriving from V_{NN} a low-momentum potential $V_{\text{low-k}}$ defined within a cutoff momentum Λ . This is a smooth potential which preserves exactly the onshell properties of the original V_{NN} and is suitable for being used directly in nuclear structure calculations.

Let us now outline briefly the derivation of $V_{\text{low-k}}$ [14]. The repulsive core contained in V_{NN} is smoothed by integrating out the high-momentum modes of V_{NN} down to Λ . This integration is carried out with the requirement that the deuteron binding energy and low-energy phase shifts of V_{NN} are preserved by $V_{\text{low-k}}$. This is achieved by the following T -matrix equivalence approach.

We start from the half-on-shell T matrix for V_{NN}

$$T(k', k, k^2) = V_{NN}(k', k) + \mathcal{P} \int_0^\infty q^2 dq V_{NN}(k', q) \frac{1}{k^2 - q^2} T(q, k, k^2) \quad ,$$

where \mathcal{P} denotes the principal value and k , k' , and q stand for the relative momenta. The effective low-momentum T matrix is then defined by

$$T_{\text{low-k}}(p', p, p^2) = V_{\text{low-k}}(p', p) + \mathcal{P} \int_0^\Lambda q^2 dq V_{\text{low-k}}(p', q) \frac{1}{p^2 - q^2} T_{\text{low-k}}(q, p, p^2) \quad , \quad (5)$$

where the intermediate state momentum q is integrated from 0 to the momentum space cutoff Λ and $(p', p) \leq \Lambda$. The above T matrices are required to satisfy the condition

$$T(p', p, p^2) = T_{\text{low-k}}(p', p, p^2); \quad (p', p) \leq \Lambda. \quad (6)$$

The above equations define the effective low-momentum interaction $V_{\text{low-k}}$, and it has been shown [14] that their solution is provided by the same KLR folded-diagram expansion [6, 12] mentioned before.

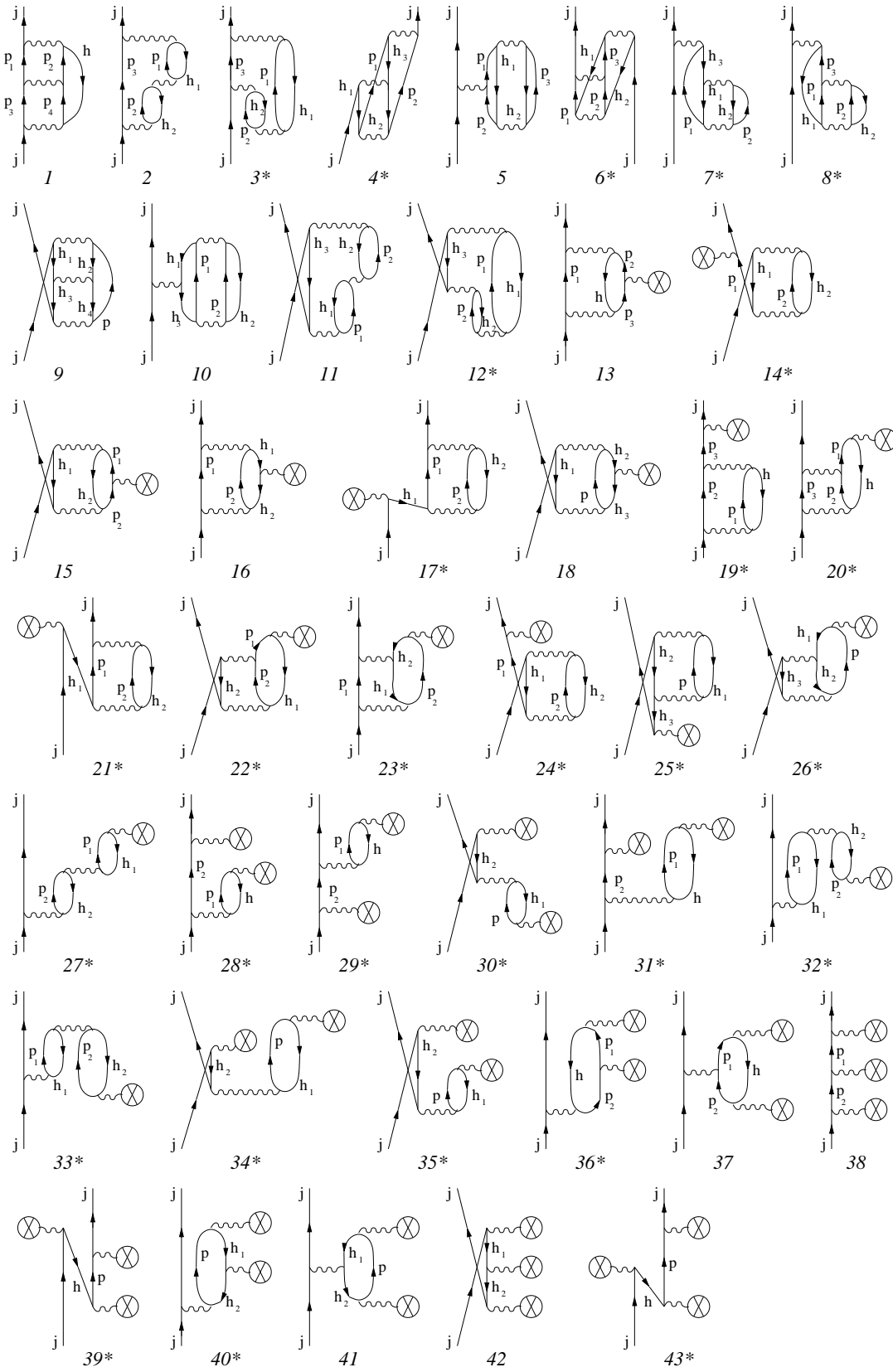


FIG. 3: Same as Fig. 2, but for third-order diagrams.

In addition to the preservation of the half-on-shell T matrix, which implies preservation of the phase shifts, this $V_{\text{low-}k}$ preserves the deuteron binding energy, since eigenvalues are preserved by the KLR effective interaction. For any value of Λ , the $V_{\text{low-}k}$ can be calculated very accurately using iteration methods. Our calculation of $V_{\text{low-}k}$ is performed by employing the iteration method proposed in [15], which is based on the Lee-Suzuki similarity transformation [13].

We have derived from the high-precision CD-Bonn NN potential [10] a class of $V_{\text{low-}k}$'s corresponding to values of the cutoff Λ ranging from 2.1 to 2.6 fm^{-1} . These $V_{\text{low-}k}$'s are all onshell equivalent, more precisely they all yield the same deuteron binding energy and NN scattering data up to the anelastic threshold, which corresponds to a relative momentum $k \simeq 2.1 \text{ fm}^{-1}$, as the CD-Bonn potential. However, this does not imply that these $V_{\text{low-}k}$'s give the same results when employed in the calculation of the single-particle spectra, since the larger the value of the cutoff the more the repulsive high-momentum components are explicitly included in $V_{\text{low-}k}$. In other words, $V_{\text{low-}k}$'s corresponding to different cutoffs have different offshell behaviors (see for instance Coraggio et al. [16]). To illustrate this, let us consider the offshell tensor force strength. This is related to the D -state probability of the deuteron P_D , which implies that, when comparing $V_{\text{low-}k}$'s with different cutoffs, offshell differences are seen in P_D differences. From inspection of Table I, where the P_D 's for various $V_{\text{low-}k}$'s are reported, it can be seen that the larger the value of the cutoff the stronger the offshell tensor force.

TABLE I: Values of P_D for $V_{\text{low-}k}$'s corresponding to different cutoff momenta Λ (in fm^{-1}) compared with the value yielded by the original CD-Bonn potential.

2.1	2.2	2.3	2.4	2.5	2.6	CD-Bonn
3.96	4.09	4.21	4.32	4.41	4.49	4.85

III. RESULTS

Calculated and experimental single-particle spacings for the one-proton valence nucleus ^{133}Sb are reported in Fig. 5 as a function of the cutoff Λ . We have found it appropriate for the perturbative expansion to limit the value of Λ to 2.6 fm^{-1} , since larger values of the cutoff lead to a rapid deterioration of the convergence properties. The calculations of diagrams have been performed using intermediate states whose excitation energy is up to $N_{\text{max}} = 15$ harmonic-oscillator quanta, so to obtain the stability of the results within few tens of keV when increasing the number of intermediate particle states. This is shown in Fig. 4, where we report the relative SP energies calculated at third order in H_1 , with a cutoff value $\Lambda = 2.6 \text{ fm}^{-1}$, as a function of N_{max} . The oscillator parameter used is $\hbar\omega = 7.88 \text{ MeV}$, accord-

ing to the expression $\hbar\omega = 45A^{-1/3} - 25A^{-2/3}$ [17] for $A = 132$, and for protons the Coulomb force has been explicitly added to the $V_{\text{low-}k}$ potential.

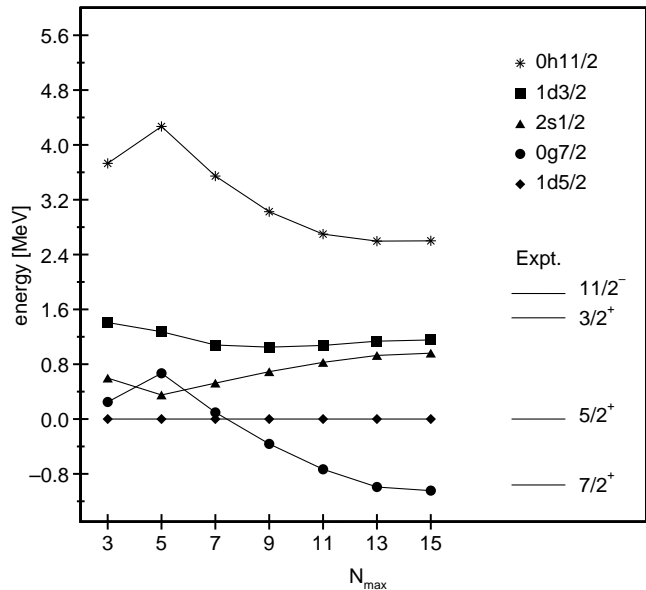


FIG. 4: Theoretical single-particle spacings in ^{133}Sb relative to the $1d_{5/2}$ level, as a function of N_{max} (see text for details). The calculations refer to a cutoff $\Lambda = 2.6 \text{ fm}^{-1}$. The experimental spectrum of ^{133}Sb is also reported.

It is important to point out that our model space is spanned by the $0g_{7/2}$, $1d_{5/2}$, $1d_{3/2}$, $2s_{1/2}$, and $0h_{11/2}$ states above the ^{132}Sn core, so we have downshifted the unperturbed energies of the $0h_{11/2}$ and $0g_{9/2}$ levels by a quantity equal to $\hbar\omega$. In this way the $2s1d0g0h$ shell is degenerate, as required by the theory of the time-dependent degenerate linked-diagram expansion, and the $0g_{9/2}$ acts as a hole state below the Fermi surface. Anyway, the inclusion of diagrams with $(V - U)$ -insertions in the \hat{Q} box assures that our results are perturbatively independent of the choice of U . In fact, to sum up the $(V - U)$ -insertion diagrams to all orders is equivalent to employ a Hartree-Fock self-consistent basis.

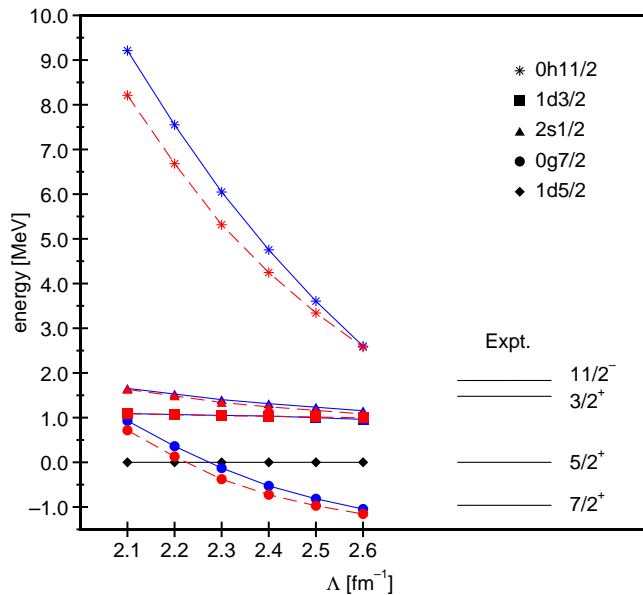


FIG. 5: (Color online) Calculated and experimental single-particle spacings in ^{133}Sb relative to the $1d_{5/2}$ level (black line), as a function of the cutoff momentum Λ . The blue lines are results at third-order in the perturbative expansion. The red dashed lines refer to results obtained with the Padé approximant [2|1] (see text for details).

The results shown in Fig. 5 (blue lines) are normalized with respect to the $0d_{5/2}$ state (straight black line) in order to evidence the changes in the spacings when increasing the cutoff Λ . In this figure, we have also reported (red dashed lines) the results obtained by calculating the Padé approximant [2|1]

$$[2|1] = \hat{Q}_0 + \hat{Q}_1 + \frac{\hat{Q}_2}{1 - \hat{Q}_3/\hat{Q}_2}, \quad (7)$$

\hat{Q}_i being the the vertex function \hat{Q} -box calculated through the i th-order in the input interaction V_{NN} . Using Padé approximants [18, 19] one may obtain an estimate of the value to which the perturbative series should converge. So the comparison between the third-order results and those obtained by means of the Padé approximant [2|1] is an indicator of the dependence of our results on the higher-order perturbative terms.

From inspection of Fig. 5, it can be seen that the calculated spin-orbit splitting between $1d_{3/2}$ and $1d_{5/2}$ levels is almost independent from Λ , the experimental separation being reasonably well reproduced. The distance between the $2s_{1/2}$ energy and the centroid of the $1d$ levels is rather independent from the cutoff too, but there is no experimental counterpart. It is worth to point out that the $1d_{3/2}$ and $2s_{1/2}$ relative energies do not exhibit a significant dependence on higher-order contributions, the difference between the third-order results and those obtained with the [2|1] Padé approximant being very small.

The situation is very different for the calculated relative energies of the $0g_{7/2}$ and $0h_{11/2}$ levels, whose spin-

orbit partners have been placed outside the chosen model space. The calculated $0g_{7/2}$, $0h_{11/2}$ relative energies show a strong dependence on the cutoff Λ and a slightly worse perturbative behavior. The most striking feature is that for small values of the cutoff the discrepancies with respect to the experimental data are quite large, while a better agreement is obtained increasing Λ . In particular, it should be pointed out that with small values of the cutoff the $0h_{11/2}$ level is far away in energy from the other levels, thus implying a shell closure at $Z = 70$. A much more reasonable spectrum of ^{133}Sb is obtained when increasing the value of the cutoff which cause the intruder $0h_{11/2}$ proton state to join the 50-82 shell. This evidences the non-negligible role of the high-momentum components of V_{NN} in the formation of the observed shell structure.

However, after these remarks one may wonder whether when increasing Λ the model space should be enlarged to include the $2p1f0h$ levels. More precisely, for large value of the cutoff it might occur a sort of “shell-quenching” when calculating the single-particle spectrum above the closed-shell ^{132}Sn . As a consequence, the $0h_{11/2}$ state as well as its parity partners ($0h_{9/2}$, $1f_{7/2}$, $1f_{5/2}$, $2p_{3/2}$, $2p_{1/2}$) would approach in energy the $2s1d0g$ states, leading to the birth of a sort of “macro”-shell $2s1d0g2p1f0h$.

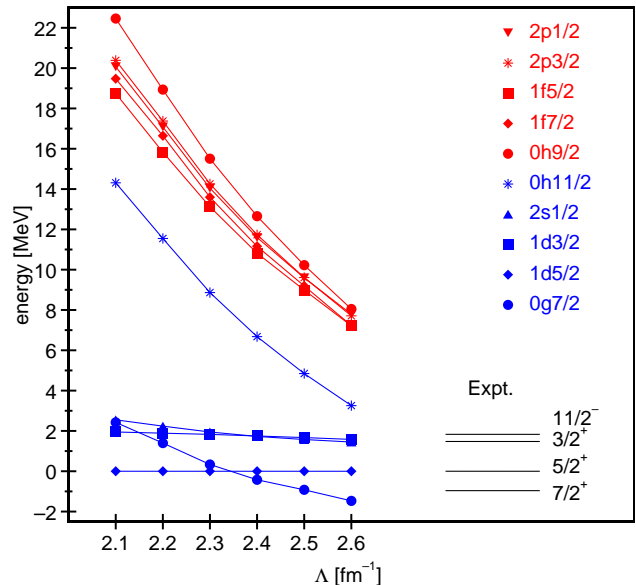


FIG. 6: (Color online) Calculated and experimental single-particle spacings in ^{133}Sb relative to the $1d_{5/2}$ level (black line), as a function of the cutoff Λ . The blue lines denote the $2s1d0g0h$ levels, while the red one the $2p1f0h$ levels (see text for details).

In order to investigate this question, we have performed a kind of theoretical “experiment”. We have carried out calculations where the $2p1f0h$ proton-particle unperturbed energies have been considered degenerate

with the $2s1d0g$ ones, and then we have turned on the interaction H_1 . The calculated energies relative to the $0d_{5/2}$ level are reported in Fig. 6. It can be seen that the spin-orbit splittings of the $2p1f0h$ levels are practically independent of the cutoff Λ , while the $0h_{11/2}$ level is pushed down from its parity partners. In particular, for large value of the cutoff the $0h_{11/2}$ state is much closer in energy to the $2s1d0g$ levels, confirming the reliability of a model space spanned only by the five $2s1d0g0h$ states.

We have found it interesting to investigate the counterpart of the $2s1d0g0h$ shell for neutrons, namely the single-particle spectrum of ^{101}Sn . In such a case, the closed-shell core is the exotic $N = Z$ nucleus ^{100}Sn . To this end, we have performed the same calculation as for ^{133}Sb , except that the harmonic-oscillator parameter is $\hbar\omega = 8.55$ MeV.

In Fig. 7 we report the calculated and experimental single-neutron energies for ^{101}Sn relative to the $1d_{5/2}$ state as a function of the cutoff Λ . As can be seen, the main difference with respect to the results shown in Fig. 5 relies in the convergence properties of the $0g_{7/2} - 1d_{5/2}$ spacing, that is the only spacing observed in ^{101}Sn . More precisely, for the $0g_{7/2}$ energy level in ^{101}Sn we have found that the third-order contributions of diagrams (27), (32), and (33) of Fig. 3, with respect to the second order diagram (3) of Fig. 2, are larger than what has been found for ^{133}Sb . All these graphs represent the so-called Tamm-Dancoff plus Random-Phase Approximation diagrams.

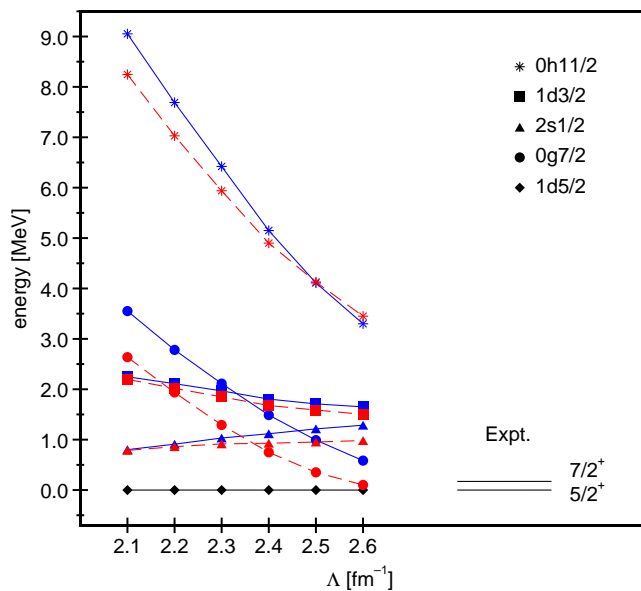


FIG. 7: (Color online) Same as in Fig. 5, but for ^{101}Sn

The stronger role of higher-order perturbative terms in the linked-diagram expansion is probably due to the fact that ^{100}Sn is a much “softer” core than ^{132}Sn .

Apart these concerns about the perturbative behavior of the linked-diagram expansion, our results confirm the need of the high-momentum components of the nuclear force in order to improve the description of the neutron shell structure.

IV. SUMMARY AND CONCLUSIONS

In this paper, we have calculated the single-particle spectra of ^{133}Sb and ^{101}Sn within the framework of the time-dependent degenerate linked-diagram perturbation theory. To investigate how the high-momentum components of the NN potential influence the structure of the proton/neutron- $2s1d0g0h$ shell, we have employed a class of onshell-equivalent realistic nucleon-nucleon potentials. These potentials have been derived from the high-precision CD-Bonn interaction [10] by way of the so-called $V_{\text{low-k}}$ approach, varying the cutoff momentum from 2.1 up to 2.6 fm^{-1} .

The perturbative behavior of the calculated single-particle relative energies is quite good for ^{133}Sb , while is less satisfactory for ^{101}Sn . This may be traced to the higher degree of exoticity of ^{101}Sn , which is very close to the proton drip line.

Our results show that, while the calculated spin-orbit splittings are scarcely dependent on the cutoff value, the relative energy of the intruder $0h_{11/2}$ state is strongly sensitive to the explicit inclusion of the high-momentum components of the NN potential. We have found that for small values of the cutoff the $0h_{11/2}$ level lies far away in energy from the other single-particle levels, while the correct shell structure is restored when increasing the cutoff.

However, it should be noted that the lack of the high-momentum components could be compensated by the inclusion of an effective three-body force [20, 21], which, for small cutoffs, may play a non-negligible role in determining the single-particle spectrum [22].

Acknowledgments

This work was supported in part by the Italian Ministero dell’Istruzione, dell’Università e della Ricerca (MIUR), by the U.S. DOE Grant No. DE-FG02-88ER40388.

- [1] T. Otsuka, T. Suzuki, R. Fujimoto, H. Grawe, and Y. Akaishi, Phys. Rev. Lett. **95**, 232502 (2005).
 [2] T. Otsuka, T. Matsuo, and D. Abe, Phys. Rev. Lett. **97**,

162501 (2006).

- [3] B. A. Brown, T. Duguet, T. Otsuka, D. Abe, and T. Suzuki, Phys. Rev. C **74**, 061303(R) (2006).

- [4] M. Zalewski, J. Dobaczewski, W. Satuła, and T. R. Werner, Phys. Rev. C **77**, 024316 (2008).
- [5] J. Dobaczewski, N. Michel, W. Nazarewicz, M. Płoszajczak, and J. Rotureau, Prog. Part. Nucl. Phys. **59**, 432 (2007).
- [6] T. T. S. Kuo and E. Osnes, *Lecture Notes in Physics, vol. 364* (Springer-Verlag, Berlin, 1990).
- [7] N. I. Kassis, Nucl. Phys. A **194**, 205 (1972).
- [8] E. Maglione and L. S. Ferreira, Phys. Rev. C **50**, 1240 (1994).
- [9] Y. Y. Sharon, M. S. Fayache, Y. D. Devi, L. Zamick, and H. Müther, Phys. Rev. C **63**, 014303 (2001).
- [10] R. Machleidt, Phys. Rev. C **63**, 024001 (2001).
- [11] S. Bogner, T. T. S. Kuo, and L. Coraggio, Nucl. Phys. A **684**, 432c (2001).
- [12] T. T. S. Kuo, S. Y. Lee, and K. F. Ratcliff, Nucl. Phys. A **176**, 65 (1971).
- [13] K. Suzuki and S. Y. Lee, Prog. Theor. Phys. **64**, 2091 (1980).
- [14] S. Bogner, T. T. S. Kuo, L. Coraggio, A. Covello, and N. Itaco, Phys. Rev. C **65**, 051301(R) (2002).
- [15] F. Androzzi, Phys. Rev. C **54**, 684 (1996).
- [16] L. Coraggio, A. Covello, A. Gargano, N. Itaco, T. T. S. Kuo, and R. Machleidt, Phys. Rev. C **71**, 014307 (2005).
- [17] J. Blomqvist and A. Molinari, Nucl. Phys. A **106**, 545 (1968).
- [18] G. A. Baker and J. L. Gammel, *The Padé Approximant in Theoretical Physics*, vol. 71 of *Mathematics in Science and Engineering* (Academic Press, New York, 1970).
- [19] N. Ayoub and H. A. Mavromatis, Nucl. Phys. A **323**, 125 (1979).
- [20] A. Schwenk and A. P. Zuker, Phys. Rev. C **74**, 061302 (2006).
- [21] G. Hagen, T. Papenbrock, D. J. Dean, A. Schwenk, A. Nogga, M. Włoch, and P. Piecuch, Phys. Rev. C **76**, 034302 (2007).
- [22] L. Coraggio, A. Covello, A. Gargano, N. Itaco, T. T. S. Kuo, D. R. Entem, and R. Machleidt, Phys. Rev. C **75**, 024311 (2007).